

# BROADBAND RING-SHAPED PMUTS BASED ON AN ACOUSTICALLY INDUCED RESONANCE

Benjamin E. Eovino<sup>1</sup>, Sina Akhbari<sup>2</sup>, and Liwei Lin<sup>1</sup>

<sup>1</sup>University of California, Berkeley, CA, USA

<sup>2</sup>Invensense Inc., San Jose, CA, USA

## ABSTRACT

We report on the principle and broadband operation of ring-shaped piezoelectric micromachined ultrasonic transducers (pMUTs) in liquid-coupled operation. Specifically, fabricated devices are measured to have a velocity bandwidth of up to 160%, which is more than 60% greater than the highest bandwidth of any reported pMUT and is tunable by altering device dimensions. This broadband performance is due to a resonance peak that is induced by acoustic interactions with the surrounding medium and occurs due to the ring-shaped geometry. Such an increased and tunable bandwidth should improve the axial resolution and efficiency of pMUTs, and possibly enable new applications such as harmonic imaging.

## INTRODUCTION

Due to the success of numerous recent research efforts, micromachined ultrasonic transducers (MUTs) continue to gain traction as a platform technology in a host of new and developed fields alike, including medical imaging, fingerprint scanning, and therapeutics [1]-[3]. Typically classified by their transduction mechanism, capacitive (cMUTs) and piezoelectric (pMUTs) are the two most prevalent technologies in the field. In contrast to cMUTs, pMUTs offer the critical advantages of being capable of relatively large displacements by eliminating thin capacitive transduction gaps, and obviating the need for large bias voltages, thereby reducing circuit and hardware complexity. Nonetheless, pMUTs remain limited by their low bandwidth; values of 26% and 43% were reported in [4] and [5], respectively, which are typical for liquid-coupled devices. It would be strongly favorable to achieve wider bandwidths, however, as the axial resolution of pMUTs operating in pulse-echo mode (e.g., for imaging applications) is dictated by the bandwidth, and pMUTs with narrow bandwidths have inherently inefficient mechanoacoustic transduction. Low-bandwidth devices also preclude many applications, such as those involving chirp waveforms or harmonic responses.

As such, the topic of increasing the bandwidth of pMUTs has garnered much attention in recent years. For example, a bandwidth of 55% was achieved with an array of individual pMUTs with different sizes and resonance frequencies, which behaved similarly to mechanically coupled resonators [6]. Such behavior has also been observed in arrays of pMUTs with equal sizes, as a 167% bandwidth was reported in [2], but array implementations with burdensome wafer footprints are required nonetheless. Conversely, a rectangular pMUT with multiple overlapping resonance modes showed a 97% bandwidth, which is the highest reported value for a standalone device [7]. This increased bandwidth was

based on acoustically inefficient higher-order vibration modes that have low volume velocities, however, and also requires very long pMUTs in order to achieve sufficiently overlapping modes [8].

In contrast to the aforementioned works, we herein report on the ring-shaped pMUT (r-pMUT) as a broadband device. Through Finite Element Analysis (FEA) simulations in COMSOL Multiphysics, the r-pMUT is shown to have two distinct resonances: the primary resonance, which has been the topic of previous reports [9], and a newfound acoustically induced resonance. A pressure integral is introduced to show that the latter of the resonances is caused by the acoustic load reaching a minimum at a specific frequency, which is defined by the device size and surrounding medium. This is substantiated by the testing of aluminum nitride (AlN) r-pMUTs in different liquid mediums, showing a bandwidth of up to 160%, which is more than 60% greater than the highest bandwidth of any reported pMUT and is tunable by altering device dimensions or liquids. Furthermore, this unprecedented bandwidth is achieved by utilizing only the acoustically efficient fundamental vibration mode and without the need for large arrays.

## CONCEPT AND OPERATING PRINCIPLE

### Overview of the Ring-shaped pMUT

Figure 1 shows a cross-sectional schematic of a vibrating r-pMUT, which consists of an annular diaphragm that is mechanically anchored by a rigid center post and bulk substrate, such that the topographic geometry of the diaphragm can be characterized by the mean radius  $r_0$  and width  $w$ . The diaphragm is composed of a bottom (inactive) AlN layer, and a top (active) AlN layer that is sandwiched between two metal electrodes, the bottom of which has full coverage and the top of which has a 55% areal coverage and is centered on the diaphragm in order to maximize electromechanical transduction efficiency [9]. When a voltage is applied between the electrodes, a transverse stress is induced in the active layer due to the  $d_{31}$  piezoelectric effect, which in turn generates a bending moment and causes the diaphragm to deflect.

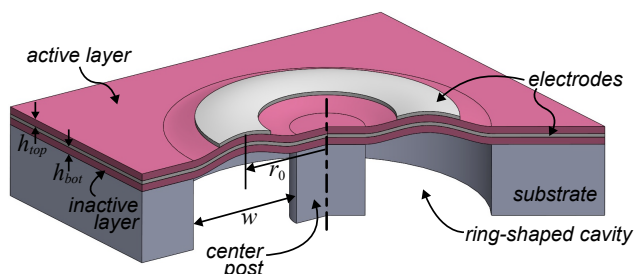


Figure 1: Cross-sectional schematic of the (deformed) ring-shaped pMUT.

## pMUT Response in Air and Liquid

We have previously reported on the performance of r-pMUTs operated in air [9], however the corresponding liquid-coupled performance has not yet been investigated. To this end, FEA simulations, which were previously shown to correlate well with observed device performance, were performed with both air and liquid environments for comparison purposes. Figure 2 shows the results of these simulations for devices with  $h_{top} = 0.8 \mu\text{m}$ ,  $h_{bot} = 1 \mu\text{m}$ ,  $w = 100 \mu\text{m}$ , and various  $r_0$  with (a) air ( $\rho = 1.2 \text{ kg/m}^3$ ,  $c = 343 \text{ m/s}$ ), and (b) Fluorinert FC-84 ( $\rho = 1730 \text{ kg/m}^3$ ,  $c = 543 \text{ m/s}$ ) as the acoustic medium, where  $\rho$  and  $c$  are the respective density and sound speed.

Air-coupled r-pMUTs (Figure 2a) typically exhibit resonance frequencies and vibration amplitudes that do not significantly change as  $r_0$  is varied at fixed  $w$ , and the devices exhibit a fairly narrow bandwidth (~1%). As shown in Figure 2b, however, the behavior of r-pMUT can differ significantly when operated in liquid as compared to in air. Paralleling the effects observed in standard MUT architectures, the additional mass and resistive loading provided by the liquid acoustic medium result in a downshift in resonance frequency and decrease in resonance amplitude, respectively. In contrast to typical pMUTs, however, accordingly designed r-pMUTs can exhibit two distinct resonance peaks; the frequency of the first (primary) resonance is largely insensitive to  $r_0$  and is analogous to the resonance seen in air-coupled r-pMUTs,

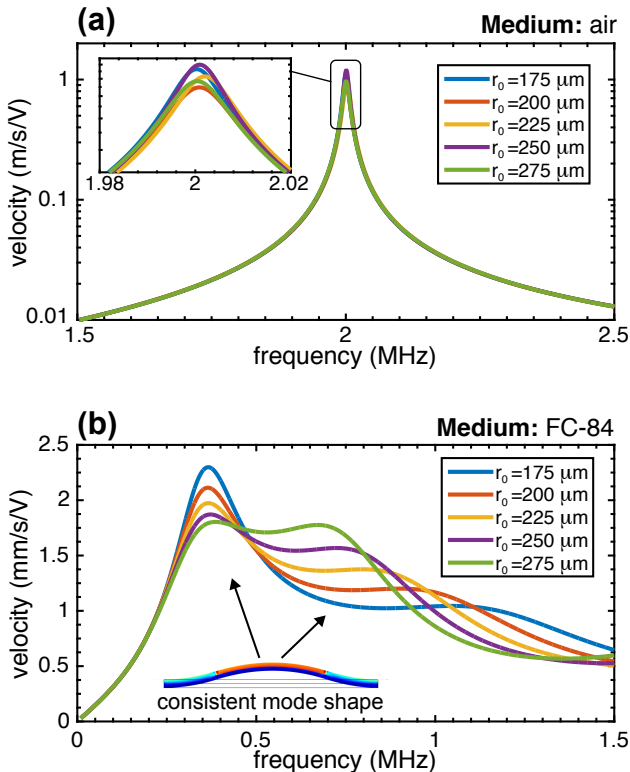


Figure 2: Simulated frequency response of ring-shaped pMUTs with  $w=100 \mu\text{m}$  and varying  $r_0$  in (a) air and (b) liquid (FC-84). Liquid-coupled devices show two distinct resonances; both have the same mode shape, and the second is more pronounced when frequency-matched with the first.

while the second resonance decreases in frequency with  $r_0$  and is more pronounced when frequency-matched with the first. Furthermore, simulations indicate that the mode shapes of both resonances are nearly identical as shown in the inset of Figure 2b, implying that the second resonance is not caused by the onset of a higher-order vibration mode, as is often the case for transducers that exhibit multiple resonances. Instead, the second resonance is in fact caused by interactions with the acoustic medium.

## Acoustic Resonance

As a pMUT vibrates in the presence of an acoustic medium, it generates a pressure that imparts a force back on the diaphragm and therefore affects the dynamics of the device. In order to demonstrate that acoustic interactions are the cause of the second resonance observed in r-pMUT, we begin by approximating the diaphragm as a thin vibrating ring with radius  $r_0$ , as shown in Figure 3a. We then express the acoustic pressure at an arbitrary angle  $\theta$  generated by an infinitesimal point source that generates a pressure  $p_0$  as

$$p_a(\theta) = \frac{p_0}{2r_0 \sin(\theta/2)} \cos(2kr_0 \sin(\theta/2)), \quad (1)$$

where  $k = 2\pi/\lambda = 2\pi f/c$  is the acoustic wavenumber. Using the acoustic properties of FC-84, this frequency-dependent pressure is then numerically integrated along the ring, normalized, and plotted in Figure 3b. It should be noted that Eq. 1 has a singularity at  $\theta = 0$ , and therefore the lower integration limit is arbitrarily set to  $1^\circ$ , however the shape and periodicity of the resulting integral is insensitive to this lower bound provided it is less than  $5^\circ$ . In Figure 3b it is apparent that there are distinct frequencies at which the pressure integral, and therefore the acoustic loading, is minimized; the first local minimum occurs at about  $f = 1.07 \text{ MHz}$  for  $r_0 = 175 \mu\text{m}$ , and decreases in frequency with increasing  $r_0$ . Such pronounced trends in the acoustic loading are unique to the ring-shaped design and play a significant role in the behavior of r-pMUTs. As shown in Figure 3c, the frequency of the first local minimum in the pressure integral occurs at about  $kr_0 = 2.1$ , and shows the same trend and is highly correlated with the frequency of the second resonance from Figure 2b. Indeed, at frequencies in which the acoustic loading is significantly reduced, the pMUT is able to achieve higher velocities, which is manifested in the frequency response as an additional resonance peak.

Understanding the cause of the second resonance has powerful implications for r-pMUT design and utility. Firstly, it allows for recognition of the independent effects of the device geometry parameters: the film stack and  $w$  determine the primary resonance frequency, and  $r_0$  sets the frequency of the second resonance. This facilitates tailored designs and enables the targeting of a range of bandwidths and/or amplitudes. On a different note, because the second resonance is induced by interactions with the acoustic medium, it is also an indicator of strong coupling and efficient mechanoacoustic transduction, which is a primary function of a pMUT.

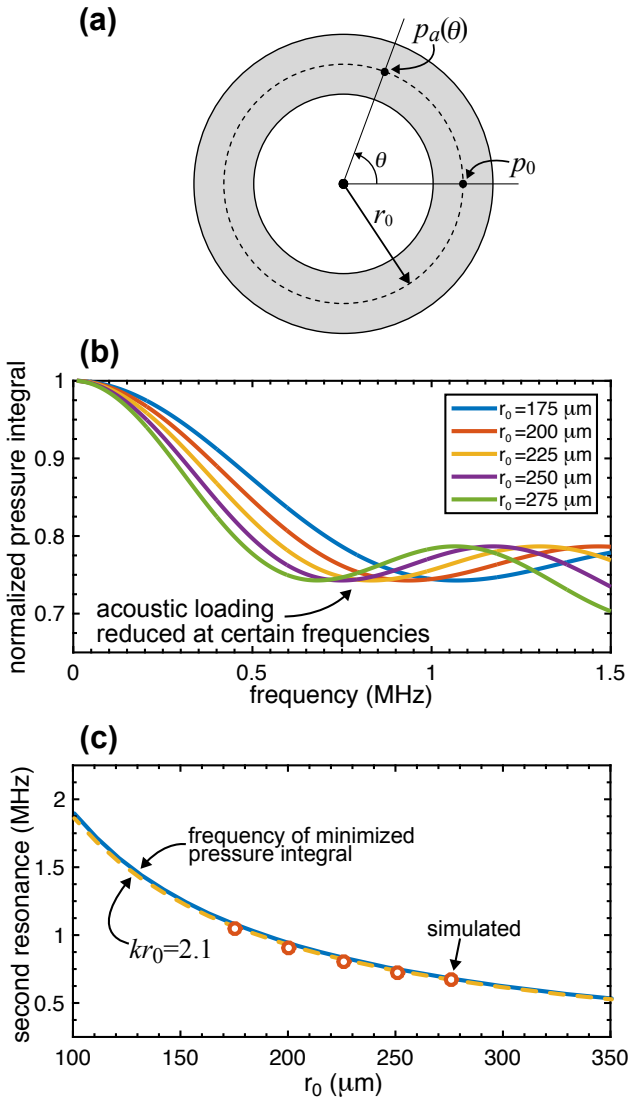


Figure 3: (a) Approximation of the ring-shaped pMUT as a thin ring at  $r_0$ , used to integrate the pressure from a point source  $p_0$  around the ring; (b) normalized pressure integral, showing reduced loading at specific frequencies; (c) comparison of simulated and predicted second resonance frequencies, evidencing acoustic interactions as the cause of the second resonance.

## EXPERIMENTAL VERIFICATION

### Methods

An optical image of the r-pMUTs used in testing is provided in Figure 4a. The fabrication has been covered in our previous work [9], and the diaphragm is composed of an AlN (1000 nm)/Mo (130 nm)/AlN (800 nm)/Mo (130 nm) film stack. The device chip contains 8 r-pMUTs with a designed width of  $w = 90 \mu\text{m}$  and various  $r_0$ , and is mounted on a custom PCB for electrical connections. For performance characterization, the frequency response of the devices is measured using a laser Doppler vibrometer (LDV, OFV-5000, Polytec Inc.) as shown in Figure 4b, where the velocity is measured at the center of the vibrating diaphragm (i.e., at  $r_0$ ). In order to examine the effect of the acoustic medium on the frequency response, the test fixture is filled with various liquid acoustic media.

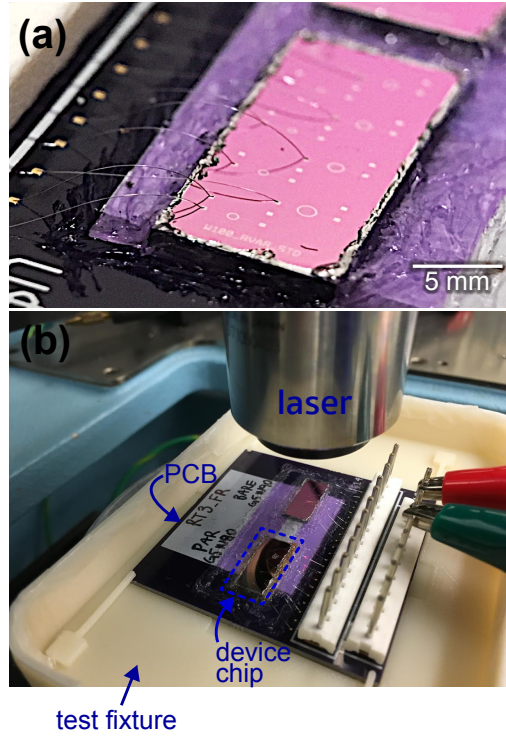


Figure 4: (a) optical image of the r-pMUT chip with the devices used for testing mounted on a PCB, and (b) test setup used to measure the frequency response with LDV. The test fixture is filled with different liquids in order to examine their effect on the frequency response.

### Results and Discussion

Figure 5 displays the results of the LDV measurements of the same devices in both Fluorinert (a) FC-40 ( $\rho = 1190 \text{ kg/m}^3$ ,  $c = 684 \text{ m/s}$ ), and (b) FC-84. The frequency response curves have been smoothed by convolving the raw data with a Gaussian (std. dev. = 20 kHz) in order to reduce the effects of the  $\lambda/4$  spurious resonances that occur due to acoustic echoes from the surface liquid/air interface, then normalized to a maximum value of 1 (0 dB). As expected, the r-pMUTs exhibit a primary resonance that is independent of mean radius regardless of the acoustic medium. In contrast, the fractional bandwidth, defined as the -6 dB frequency range divided by the resonance (maximum velocity) frequency (i.e.,  $BW_f = \Delta f/f_0$ ), varies significantly according to the acoustic medium and device size. When the acoustic medium is FC-40,  $BW_f$  varies between 57% and 68% for the smallest and largest r-pMUT tested, respectively, as shown in Figure 5a. While the normalized center velocity does increase with  $r_0$ , the  $BW_f$  does not drastically change because the acoustic resonance occurs at  $f > 780 \text{ kHz}$  for all  $r_0$ , thus the two resonances are not sufficiently matched to have a pronounced effect. Conversely, the reduced sound speed in FC-84 lowers the acoustic resonance frequency, such that it is expected to occur at  $f = 620 \text{ kHz}$  for  $r_0 = 300 \mu\text{m}$ . This matches well with measurements in Figure 5b, where a broad secondary peak near 600 kHz is present for  $r_0 = 300 \mu\text{m}$ . Indeed, with FC-84 as the acoustic medium, the r-pMUTs tested showed a bandwidth that is tunable from 65% to as high as 160%, which is a marked improvement over the

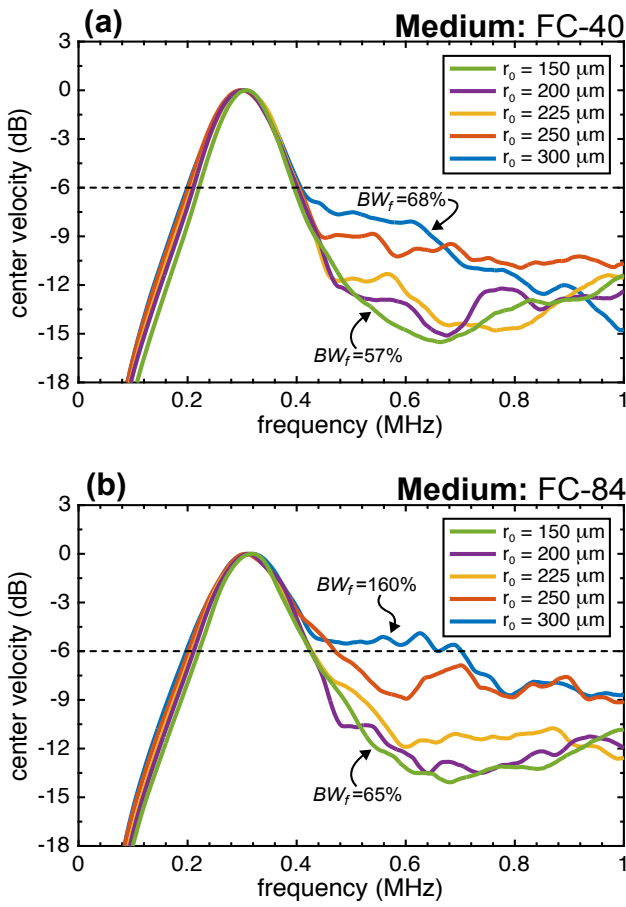


Figure 5: Measured frequency response of ring-shaped pMUTs in (a) FC-40 and (b) FC-84. FC-40 has a higher sound speed, so the acoustic resonance is not matched to the first resonance, and we see only minor changes as  $r_o$  is increased. In FC-84, however, the acoustic resonance is at 620 kHz for  $r_o=300\mu\text{m}$ , and therefore has a strong effect. In this case, a bandwidth of 160% is achieved.

previously reported maximum bandwidth for a standalone pMUT of 97%.

## CONCLUSION

We have explored the ring-shaped pMUT (r-pMUT) as a broadband device with tunable performance. Two distinct resonances have been observed: the first is the well-understood resonance of the fundamental vibration mode, and the second is due to the frequency-dependent acoustic loading. Owing to the fact that each resonance is affected by different geometric device parameters, one can readily select the proper device size to achieve the desired bandwidth for a given application. In fact, with an accordingly designed r-pMUT, testing shows that a bandwidth as high as 160% is achievable, and analysis indicates that still wider bandwidths are feasible. This indicates that r-pMUTs are a candidate to improve the efficiency and resolution of pMUT-based systems in many fields. Furthermore, as high-performance MUT design is typically limited to material or mechanical-domain improvements, this work opens up a new direction to include acoustic considerations.

## ACKNOWLEDGEMENTS

This work was supported in part by the Tsinghua-Berkeley Shenzhen Institute (TBSI) and by the National Science Foundation Graduate Research Fellowship Program under Grant No. DGE 1106400. The authors would also like to thank Xiaoyue Jiang and Levent Beker for helpful discussions, along with Qi Wang for assistance with LDV measurements.

## REFERENCES

- [1] D. Stephens *et al.*, "First in vivo use of a capacitive micromachined ultrasound transducer array-based imaging and ablation catheter," *Journal of Ultrasound in Medicine*, vol. 31, no. 2, pp. 247-256, 2012.
- [2] S. Akhbari *et al.*, "Bimorph piezoelectric micromachined ultrasonic transducers," *Journal of Microelectromechanical Systems*, vol. 25, no. 2, pp. 326-336, 2016.
- [3] X. Jiang *et al.*, "Monolithic 591x438 DPI ultrasonic fingerprint sensor," in *2016 IEEE 29th International Conference on Micro Electro Mechanical Systems (MEMS)*, pp. 145-148, Shanghai, China.
- [4] Y. Lu *et al.*, "High frequency piezoelectric micromachined ultrasonic transducer array for intravascular ultrasound imaging," in *2014 IEEE 27<sup>th</sup> International Conference on Micro Electro Mechanical Systems (MEMS)*, San Francisco, pp. 745-748.
- [5] J. Jung *et al.*, "Fabrication of a two-dimensional piezoelectric micromachined ultrasonic transducer array using a top-crossover-to-bottom structure and metal bridge connections," *Journal of Micromechanics and Microengineering*, vol. 23, Dec. 2013, pp. 1-9.
- [6] A. Hajati *et al.*, "Three-dimensional micro electromechanical system piezoelectric ultrasound transducer," *Applied Physics Letters*, vol. 101, no. 25, art. no. 253101, Dec. 2012.
- [7] Y. Lu *et al.*, "Broadband piezoelectric micromachined ultrasonic transducers based on dual resonance modes," in *2015 IEEE 28<sup>th</sup> International Conference on Micro Electro Mechanical Systems (MEMS)*, pp. 146-149, Estoril, Portugal.
- [8] T. Wang, T. Kobayashi, and C. Lee, "Micromachined piezoelectric ultrasonic transducer with ultra-wide frequency bandwidth," *Applied Physics Letters*, vol. 106, no. 1, art. no. 013501, 2015.
- [9] B. Eovino, S. Akhbari, and L. Lin, "Ring-shaped piezoelectric micromachined ultrasonic transducers (PMUT) with increase pressure generation," in *Solid-state Sensor and Actuator Workshop (Hilton Head)*, pp. 432-435, 2016.

## CONTACT

\*B. Eovino, tel: +1-408-4107375; beovino@berkeley.edu